Key Points:
- The tropopause-level, polar, and subtropical jet streams are becoming increasingly wavy during Northern Hemisphere winter
- Despite the increase in waviness, the speed of the jets has remained nearly constant
- The polar jet is slowly, but systematically, creeping poleward in accord with climate model projections

Correspondence to:
J. E. Martin,
jemarti1@wisc.edu

Recent Trends in the Waviness of the Northern Hemisphere Wintertime Polar and Subtropical Jets

Jonathan E. Martin[1] 📧

[1]Department of Atmospheric and Oceanic Sciences, University of Wisconsin-Madison, Madison, WI, USA

Abstract A feature-based metric of the waviness of the wintertime, Northern Hemisphere polar, and subtropical jets is developed and applied to three different reanalysis data sets. The analysis first identifies a "core isertel" along which the circulation per unit length is maximized in the separate polar (315:330K) and subtropical (340:355K) jet isentropic layers. Since the core isertel is, by design, an analytical proxy for the respective jet cores, the waviness of each jet is derived by calculating a hemispheric average of the meridional displacements of the core isertel from its equivalent latitude—the southern extent of a polar cap whose area is equal to the area enclosed by the core isertel. Analysis of the seasonal average waviness over the time series of the various data sets reveals that both jets have become systematically wavier while exhibiting no trends in their average speeds. The waviness of each jet evolves fairly independently of the other in most cold seasons and the slow northward creep of the polar jet is statistically significant. Finally, comparison of the composites of the waviest and least wavy seasons for each species reveals that such interannual variability is manifest in familiar large-scale circulation anomalies.

Plain Language Summary Among the most common structural features of the earth's atmosphere are the narrow, meandering ribbons of maximum wind speed known as the jet streams. On any given winter day, there are usually two such jet streams; one located at ~9 km (the polar jet) and another, further south, located at ~12 km (the subtropical jet). These jet streams are both important weather producing features as well as influential governors of regional climate. This study considers trends in the wintertime waviness of the two jets as portrayed in three different data sets with long time series. The analysis reveals three important results. First, the waviness of both jets has been systematically increasing since ~1960. Second, despite their increasing waviness, the maximum speed of both jets has hardly changed. Third, the polar jet has been creeping slowly, but persistently, poleward over the last several decades. All three of these results are consistent with predictions that have recently been made about the behavior of the jets in a warmer climate and thus offer observational support for these forecasts.

1. Introduction

Among the most ubiquitous structural features of the Earth's atmosphere are the narrow, tropopause-level wind speed maxima known as jet streams or jets. These jets, often found nearly girdling the globe while exhibiting large meridional meanders, are the primary phenomena at the interface between synoptic-scale weather systems and the large-scale circulation. Consequently, they play a substantial role in the production of sensible weather in the midlatitudes while serving as particularly influential governors of regional climate. Decades of observational work has identified two main varieties of jets, distinguished by their underlying dynamical origins. The polar jet (POLJ) forms as a result of eddy momentum flux convergence associated with the development of midlatitude baroclinic waves (e.g., Held, 1975; Panetta, 1993; Rhines, 1975) and is connected, via the thermal wind relationship, to the troposphere-deep baroclinicity of the middle latitudes. The subtropical jet (STJ) forms in response to angular momentum transport by the thermally direct Hadley circulation (Held & Hou, 1980) and is, therefore, tied to the poleward edge of the tropical Hadley Cell. As a consequence of their different origins, the POLJ and STJ are often widely separated by latitude as well as elevation. The Northern Hemisphere (NH) jet stream has centers of maximum intensity located over the western Atlantic and western Pacific Oceans with the wintertime Pacific jet extending from East Asia to the date line. Unlike the Atlantic jet, the wintertime Pacific jet is regularly characterized by a collocation (or vertical superposition) of POLJ and STJ components and thus is often a hybrid feature (e.g., Christenson et al., 2017).

Both species of jets reside near the tropopause—the thermodynamic boundary that separates the stratosphere from the troposphere. The tropopause is characterized by strong first order discontinuities in static stability, the mixing ratios of certain chemical constituents, as well as potential vorticity (PV). Importantly, the tropopause does not occur at a uniform height over the entire hemisphere nor does it exhibit a monotonic slope with latitude. Instead, as first identified by Defant and Taba (1957), there is generally a three-step structure in tropopause height from equator-to-pole with local regions of steep slope occurring at successively lower elevation with increasing latitude.

These local maxima in slope are also regions of large PV gradient on isentropic surfaces. This PV gradient serves as the restoring force for Rossby waves, the ubiquitous, planetary-scale ridge-trough couplets that are primarily responsible for the production of organized weather systems in the extratropics. Morgan and Nielsen-Gammon (1998) demonstrated the utility of maps of potential temperature (θ) and wind speed on the so-called dynamic tropopause (defined as a surface of constant Ertel, 1942 PV) for diagnosing weather systems. In this framework, the maxima in tropopause slope become regions of large PV gradient on isentropic (θ) surfaces, or large θ gradient on isertelic (constant PV) surfaces, and are theoretically (Cunningham & Keyser, 2004; Hoskins et al., 1985) and empirically (Davies & Rossa, 1998; Hoskins & Berrisford, 1988) linked to the tropopause-level jet cores.

The behavior of the jets in a warmer climate has been a topic of considerable research effort recently. The consensus view is that a robust poleward displacement of the jet axes will likely characterize a warmer world (e.g., Barnes & Polvani, 2013; Miller et al., 2006; Swart & Fyfe, 2012; Woollings & Blackburn, 2012; Yin, 2005). In addition, attempts have been made, by various methods, to assess the waviness of the midlat-
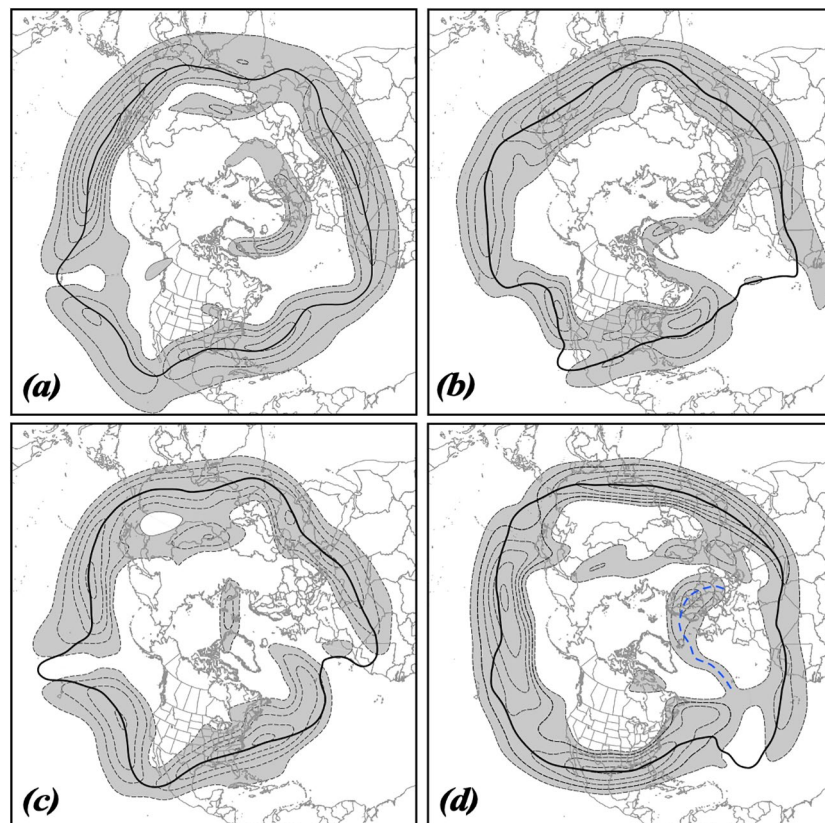

Figure 1. Isotachs of the daily average wind speed (contoured every 10 m s^{-1} and shaded above 30 m s^{-1}) and the core isertel (bold solid line) in the 340:355 K isentropic layer on (a) January 19, 1958, (b) December 26, 1968, (c) February 19, 1979, and (d) February 18, 1998. The core isertel has a value of 2.0 PVU in (a), 2.1 PVU in (b), 2.1 PVU in (c), and 1.4 PVU in (d). Blue dashed line in (d) represents a portion of the axis of the polar jet on the same day in the 315:330 K isentropic layer (see Figure 2d and text for explanation).

itude flow containing the jets. Particularly at issue in recent years has been attribution of any such changes to the enhanced lower tropospheric warming at high latitudes known as Arctic amplification (Blackport & Screen, 2020; Francis, 2017; Francis et al., 2018; Screen & Simmonds, 2010, 2013; Serreze et al., 2009; Vavrus, 2018). Nearly all such attempts have employed analysis metrics involving geopotential height contours or horizontal wind components in the middle and upper troposphere (e.g., Barnes, 2013; Chen et al., 2015; Di Capua & Coumou, 2016; Francis & Vavrus, 2012, 2015; Martineau et al., 2017). However, considered from a PV perspective, the flow at 500 hPa is often strongly influenced by near surface thermal contrasts (i.e., dynamically equivalent to low-level PV gradients following Bretherton, 1966), internal diabatic processes, and tropopause-level PV anomalies (Davis & Emanuel, 1991; Hoskins et al., 1985). Thus, though the 500 hPa flow often exhibits similarities to the jet stream flows at higher altitudes, because it is shaped by these lower tropospheric and diabatic influences to a greater extent than the tropopause-level flow, it might be expected that tropopause-level jet waviness would differ noticeably from that of the mid-troposphere. Consistent with this presumption and, despite a number of recent innovations in objective identification of the jet streams themselves (e.g., Christenson et al., 2017; Limbach et al., 2012; Manney et al., 2011; Schiemann et al., 2009), agreement on whether or not substantial changes in jet waviness have been detected does not yet exist (Barnes & Screen, 2015). Underlying this lack of consensus is the absence of a robust method of assessing the waviness of the tropopause-level jets. Without regard to the question of possible links to Arctic amplification, the goals of the present paper are limited to describing a method for separately quantifying the waviness of the subtropical and polar jets and examining recent trends in both.

The paper is organized as follows. A theoretical and observational background to the methodology used in the study is given in Section 2 along with a description of the data sets used. In Section 3, aspects of
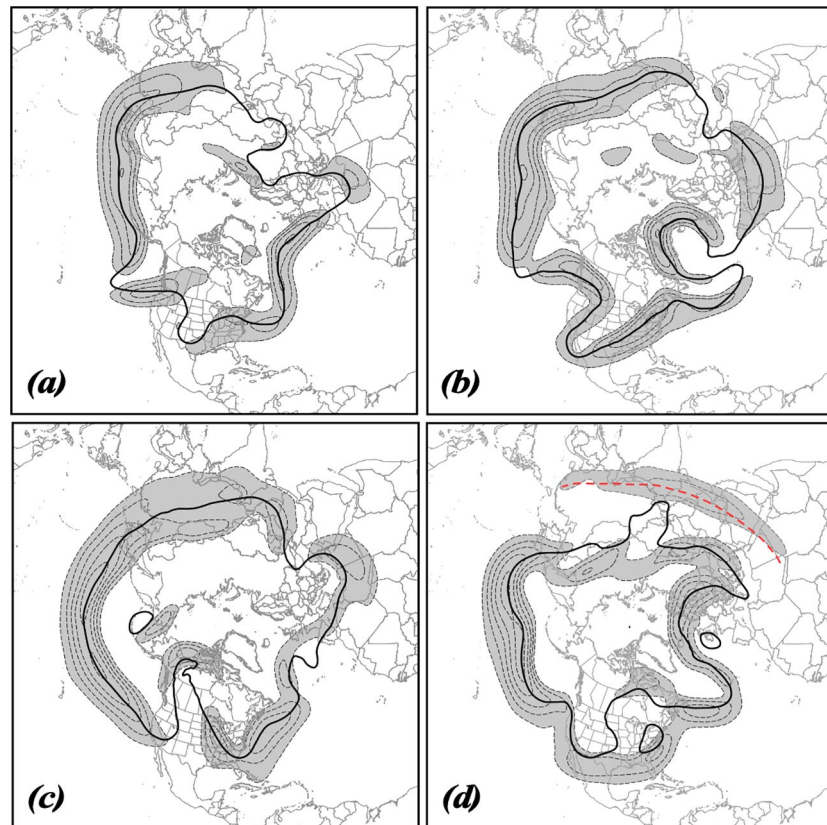

Figure 2. Isotachs of the daily average wind speed (contoured every 10 m s^{-1} and shaded above 30 m s^{-1}) and the core isertel (bold solid line) in the 315:330 K isentropic layer on (a) December 12, 1954, (b) January 8, 1967, (c) February 6, 1978, and (d) February 18, 1998. The core isertel value is 1.6 PVU in (a), 1.0 PVU in (b), 1.8 PVU in (c), and 2.2 PVU in (d). Red dashed line in (d) represents a portion of the axis of the subtropical jet on the same day in the 340:355 K isentropic layer (see Figure 1d and text for explanation).
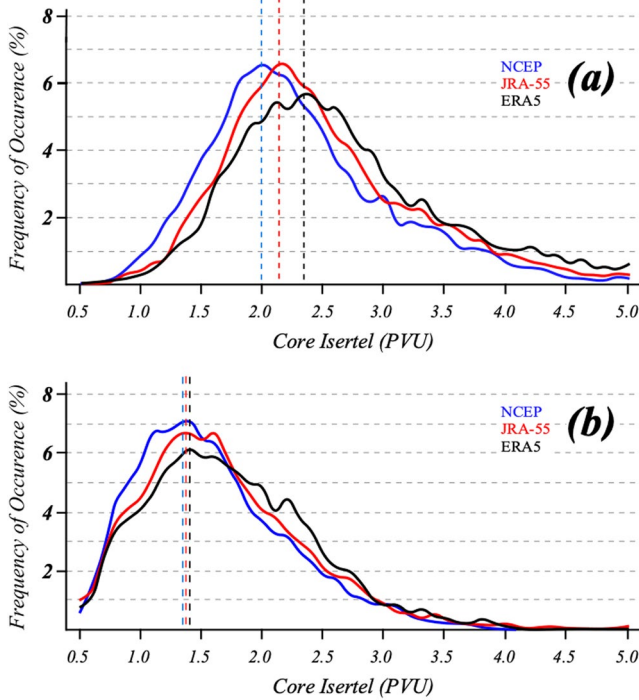
Figure 3. Frequency of occurrence of core isertel value for each reanalysis time series in (a) the 340:355 K layer and (b) the 315:330 K layer. The dashed vertical lines indicate the peak. value of the core isertel in each layer from each data set. Isertel values given in potential vorticity units (PVU, 1 PVU = 10^{-6} K m^2 kg^{-1} s^{-1}).

the long-term trend and interannual variability of the waviness of the NH, cold-season subtropical, and polar jets are considered. Included here are analyses of the differences in the composite, large-scale dynamic, and kinematic structures associated with the waviest and least-wavy cold seasons in both species of tropopause-level jets. A summary and conclusions, including suggestions for future work, are offered in Section 4.

2. Data and Methodology

In this study, the waviness of the two species of tropopause-level jets is assessed in the context of understanding their relationships to the gradient of PV in prescribed isentropic layers. Christenson et al. (2017) presented an objective method for identification of the separate polar and subtropical jets in θ/PV space. They argued that the NH cold season (NDJFM) polar (subtropical) jet core lies on the equatorward, or low PV, edge of a strong PV gradient in the 315:330 K (340:355K) isentropic layer. Justification for the PV gradient/jet relationship follows from consideration of the quasi-geostrophic potential vorticity (QGPV) following Cunningham and Keyser (2004). Recalling that QGPV is given by

$$q_g = \frac{1}{f_o}\nabla^2\varphi + f + \frac{\partial}{\partial p}\left(\frac{f_o}{\sigma}\frac{\partial\varphi}{\partial p}\right) = \Lambda(\varphi) + f$$

(where $\Lambda = \frac{1}{f_o}\nabla^2 + \frac{\partial}{\partial p}\left(\frac{f_o}{\sigma}\right)\frac{\partial}{\partial p} + \frac{f_o}{\sigma}\frac{\partial^2}{\partial p^2}$ and ϕ is the geopotential), the cross-jet gradient of QGPV ($\partial q_g/\partial n$ where $\hat{n}$ is the cross-flow direction in natural coordinates) can be expressed as

$$\frac{\partial q_g}{\partial n} = \Lambda\left(\frac{\partial\varphi}{\partial n}\right) = \Lambda\left(-fV_g\right). \tag{1}$$

after substituting from the natural coordinate expression for the geostrophic wind. Thus, local maxima in the cross-flow gradient of QGPV are collocated with maxima in the geostrophic wind speed. The analysis of Davies and Rossa (1998) offers empirical justification for confident extension of this relationship to gradients in Ertel (1942) PV.

In the foregoing analysis, we employ the zonal (u) and meridional (v) winds as well as temperature (T) at 6 h intervals from three different reanalysis data sets: National Centers for Environmental Prediction/National Center for Atmospheric Research (NCEP/NCAR), JRA-55, and ERA5 reanalyses. We use 70 winters
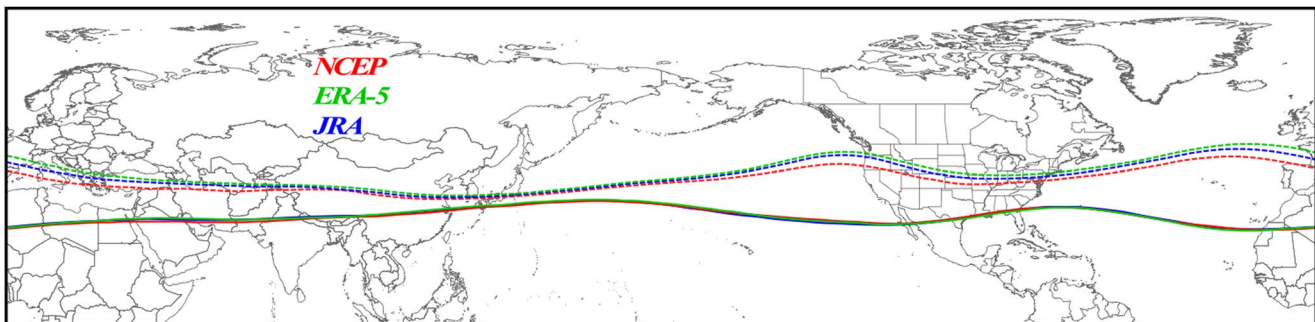

Figure 4. DJF average latitude of the core isertels of both the polar jet (dashed lines) and the subtropical jet (solid lines) from the NCEP, JRA, and ERA-5 reanalysis data sets. NCEP, National Centers for Environmental Prediction.
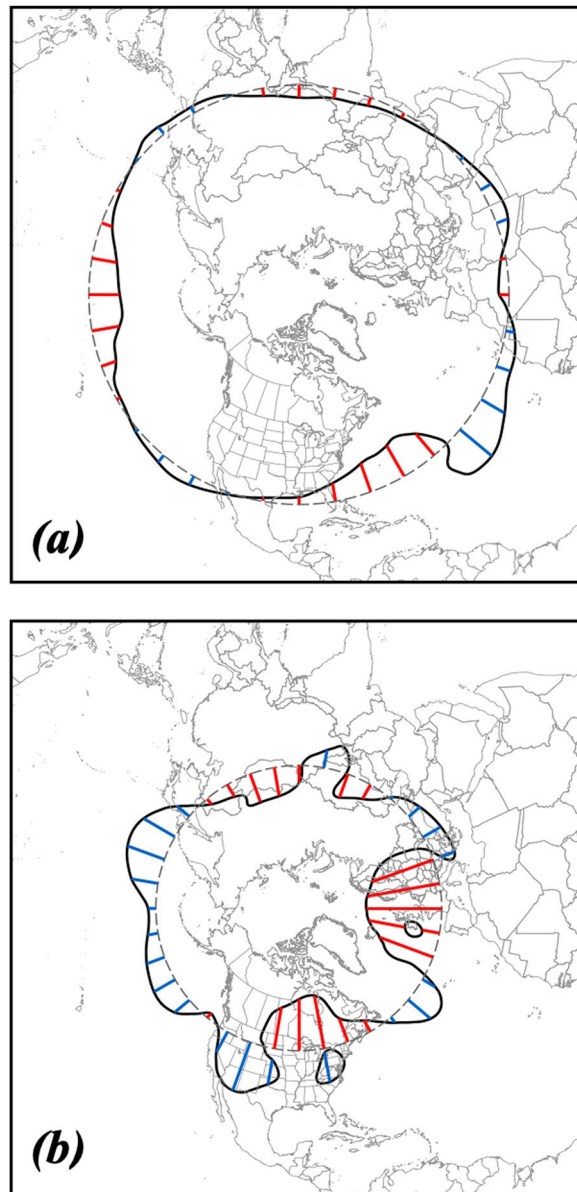
Figure 5. Schematic illustrating the concept of ALD for (a) the 340:355 K layer and (b) the 315:330 K layer on February 18, 1998. Bold black line is the core isertel in each layer (from the NCEP/NCAR Reanalysis), the gray dashed line is its equivalent latitude, and the red and blue lines represent latitudinal displacements of the core isertel poleward and equatorward of the equivalent latitude, respectively. The ALD is the average of the sum of all such segments divided by the number of such segments available in the data set. ALD, average latitudinal displacement; NCAR, National Center for Atmospheric Research; NCEP, National Centers for Environmental Prediction.

(1948–2017) of NCEP-NCAR reanalysis. The NCEP-NCAR reanalysis data are available at 17 isobaric levels to 10 hPa on a 2.5° latitude-longitude grid (Kalnay et al., 1996; Kistler et al., 2001). We employ 60 winters (1958–2017) of the Japanese 55-year (JRA-55) reanalysis with data on 60 vertical levels up to 0.1 hPa on a horizontal grid mesh of ∼55 km (Kobayashi et al., 2015). The ERA5 data are on 137 vertical levels from the surface to 80 km with grid spacing at ∼31 km covering the period from 1979 to 2017 (Copernicus Climate Change Service [CS3], 2017). The different reanalyzes are the products of varying assimilation schemes and input data sets, with some characterized by known discontinuities arising from the introduction of satellite data (e.g., Santer et al., 1999; Sturaro, 2003). Additionally, the use of data sets with variable start times can complicate the comparisons of any resulting time series. The foregoing analysis embraces these differences
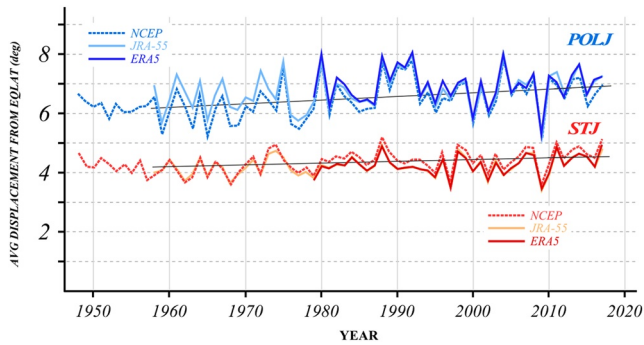
Figure 6. Seasonal average ALD (in degrees) of the NH wintertime subtropical and polar jets for each cold season in the three reanalysis time series. The polar jet values are in the three shades of blue while the subtropical jet values are in the three shades of red. The thin black line through each time series represents the trend line for each (derived from the JRA-55 data) and is significant at the 96% level. The "YEAR" on the abscissa indicates the year in which December of that cold season occurred. ALD, average latitudinal displacement; NH, Northern Hemisphere.

as evidence of, rather than impediments to, the robustness of the analysis method.

As will be shown presently, the analysis method involves assessment of the circulation which requires calculation of contour length. Consequently, fair comparison among the data sets is best made by adopting a uniform horizontal grid spacing. Therefore, all three data sets were bilinearly interpolated onto isentropic surfaces at 5-K intervals (from 300 to 370 K) and 2.5° latitude-longitude grid spacing using programs within the General Meteorological Analysis Package (GEMPAK) (The GEMPAK software details can be found at https://www.unidata.ucar.edu/software/gempak with additional information available at https://github.com/Unidata/gempak) (desJardins et al., 1991). The average PV and average zonal and meridional wind speeds in both the polar jet (315:330 K) and subtropical jet (340:355K) layers were then calculated four times daily for every day in the trio of time series.

By virtue of the fact that the jets are always located in a region of strong PV gradient, a reasonable proxy for the axis of maximum wind speed (or "core") of each jet is, on any given day, one of several isertels within the strong gradient region. We shall refer to this particular isertel as the "core isertel" and note here that it need not have the same value from one day to the next. We seek to quantify the daily departure from zonality of such core isertels in each jet layer as a means of directly assessing the waviness of the jet. In order to perform this analysis, we first consider the circulation

$$C = \oint \vec{U} \cdot d\vec{l}$$

along isertels ranging from 0.5 to 5.0 PVU (at 0.1 PVU intervals, 1 PVU = 10^{-6} m^2 K kg^{-1} s^{-1}) in each jet layer on every day in each time series. The core isertel in each layer on a given day is the isertel along which the average $\left|\vec{U}\right|$ per unit length is maximized. It is important to note that the decision to choose only one core isertel is made to facilitate construction of the jet core proxy, *not* to suggest a fundamental property of the jet itself. Examples illustrating the utility of this method for identifying the meandering cores of the subtropical and the polar jets are provided in Figures 1 and 2, respectively. Note that the "stray" jet core in Figure 1d, an isolated wind speed maxima far removed from the core isertel in the subtropical (340:355 K) layer, is actually the vertical extension of an obvious polar jet core in the underlying 315:330 K layer (Figure 2d). Conversely, the "stray" wind speed maxima over the Middle East and the Himalaya in Figure 2d is the lower portion of the subtropical jet core, identified in the 340:355 K layer (Figure 1d). Throughout the time series, a large fraction of such seemingly disconnected isotach maxima in either layer can be accounted for in a similar fashion.
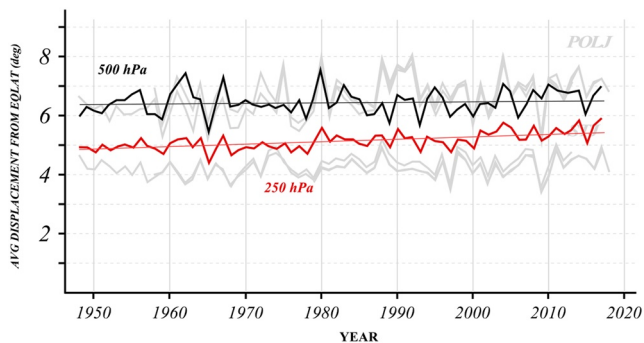

Figure 7. Seasonal average aggregate ALD (in degrees) of a set of five isohypses at 500 (solid black) and 250 hPa (solid red) from the NCEP/NCAR reanalysis data. The thin solid black line is the trend line at 500 hPa which is nearly flat and not statistically significant. The thin solid red line is the trend line at 250 hPa which indicates a more substantial trend. For comparison, the light gray shading shows the same POLJ and STJ time series shown in Figure 6. See text for additional explanation. ALD, average latitudinal displacement; NCAR, National Center for Atmospheric Research; NCEP, National Centers for Environmental Prediction; POLJ, polar jet; STJ, subtropical jet.
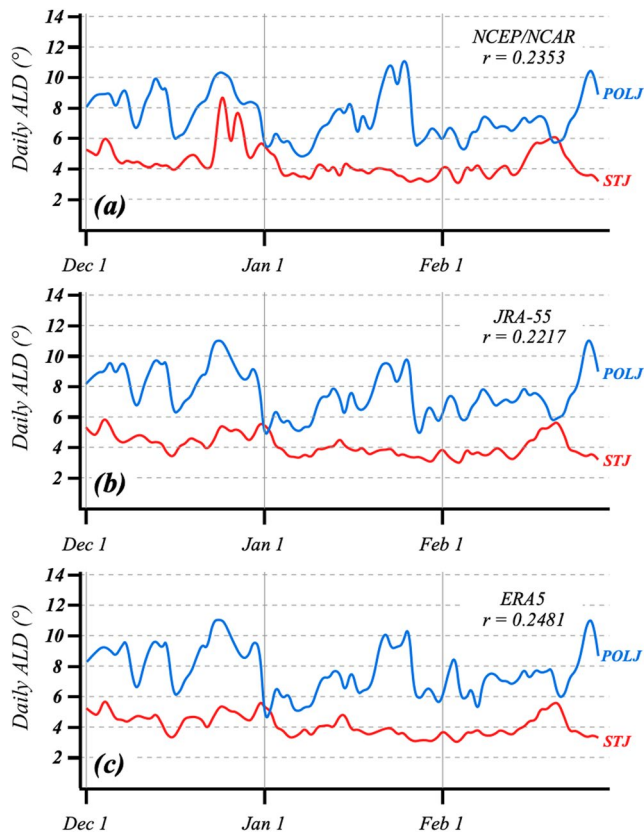
As stated earlier, the core isertel is not the same for each day in a given time series nor is it necessarily the same among the data sets on a given day that might be shared by the three time series. Consequently, its distribution in each jet layer in each data set is worthy of additional analysis. Figure 3 portrays the frequency of occurrence of the core isertels of both the subtropical and polar jets in each of the three reanalysis data sets. The core isertel of the STJ layer peaks between 2.0 and 2.4 PVU across the three different data sets with the distribution both widening and shifting toward slightly higher isertelic values from NCEP to JRA-55 and again to ERA5 (Figure 3a). Considering all three data sets, 79.4% of all DJF days exhibit a core isertel between 1 and 3 PVU in the STJ layer. The polar jet distribution is shifted toward lower PV values (Figure 3b) consistent with the concept of a "dynamically relevant PV contour" as

Figure 8. Time series of the daily ALD of the polar (blue line) and subtropical (red lines) jets from the (a) NCEP-Reanalysis, (b) JRA-55, and (c) ERA5 data sets for the cold season 1990–1991. The correlation between the two times series from each data set is indicated. ALD, average latitudinal displacement.
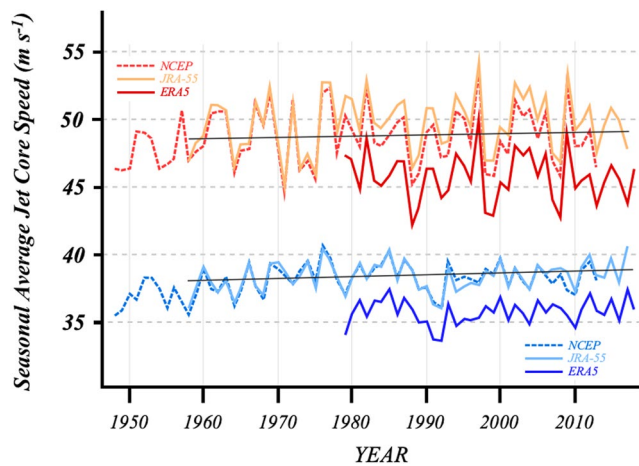

Figure 9. Seasonal average ($\bar{U}$) along the core isertel for the subtropical (red lines) and polar (blue lines) jets from each of the three reanalysis data sets. The thin black lines are trend lines for each time series from the JRA-55 data.

described by Kunz et al. (2015). A similar widening, but less shifting, of the distributions is seen in this layer where the three data sets exhibit a remarkable similarity in the peak of their core isertelic distributions. Overall, 83.6% of all DJF days had a core isertel between 1 and 3 PVU in the POLJ layer. Though the analysis employs a uniform resolution in θ space, some of the variability in the distribution of core isertels among the various data sets may be a function of differences in their native vertical resolutions as the finer resolution of the ERA5 and JRA-55 data likely impacts the location and isertelic value of the tropopause. As a separate test of the fidelity of the core isertel as a proxy for the jet cores, the DJF climatological position of the core isertel for each jet from each data set is shown in Figure 4. The proxy jet cores closely resemble those presented in prior analyses of the NH wintertime jet streams (e.g., Christenson et al., 2017; Koch et al., 2006; Manney & Hegglin, 2018; Pena-Ortiz et al., 2013).

The final step in the analysis employed here is inspired by the method developed by Huang and Nakamura (2016) to calculate the local finite-amplitude wave activity (LWA). Once the core isertel on a given day in a given layer has been identified, the area enclosed by that contour is calculated. Next, its equivalent latitude—the southern extent of a polar cap whose area is equal to the area enclosed by the core isertel—is computed. If A is the area enclosed by the core isertel at a given time, then the equivalent latitude, ϕ_e, is given by $\phi_e = \arcsin\left[1 - \dfrac{A}{2\pi R_e^2}\right]$

where R_e is the radius of the Earth. The meridional displacement of the core isertel from its equivalent latitude is then measured along each longitude line in the manner illustrated in Figure 5. For core isertels intersecting a longitude line at multiple points, only those segments of that longitude line along which the PV is greater (less) than the core isertel value south (north) of the equivalent latitude are counted. The average latitudinal displacement (ALD) of a given core isertel is then the sum of the length of all such segments divided by the number of longitude lines at the resolution of the data (e.g., $2\pi/2.5° = 144$ for the present analysis) and is converted to degrees for illustration purposes. Note that a perfectly zonal core isertel (i.e., a zonal jet) would have an ALD of 0.0 with larger numbers representing increasingly wavier jets. As an example, the ALDs of the tropopause-level jets observed on February 18, 1998 were 3.129° for the STJ (Figure 5a) and 8.893° for the POLJ (Figure 5b).

3. Analysis

3.1. Seasonal Averages

The seasonal average latitudinal displacement of each jet is calculated as a simple 90-day (no leap days) average of the daily ALD in each cold season. The results of this averaging are shown in Figure 6 and it is immediately apparent that the polar jet is substantially wavier than its subtropical counterpart. Though characterized by considerable interannual variability, both jets exhibit an increase in seasonally averaged waviness over the combined time series with $p < 0.04$ for both time series (a one-sided Student's t-test was employed) (For clarity of presentation, only the JRA-55 trend line is shown and its p-value referenced. The slope of the JRA-55 POLJ [STJ] trend is 0.009 (0.005). The 1958–2017 NCEP
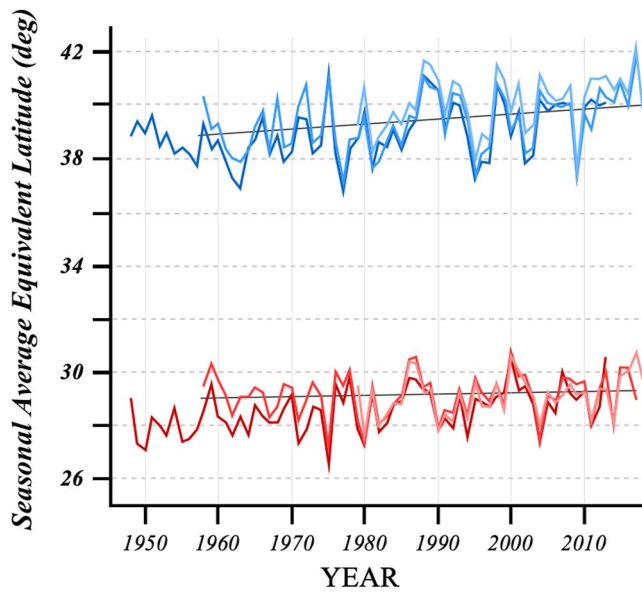
Figure 10. Time series of the seasonal average equivalent latitude of the polar (blue lines) and subtropical (red lines) jets from the three different reanalysis data sets. The thin black lines are the trend lines (from the JRA-55 data) which are small and only significant for the polar jet time series.

POLJ [STJ] trend line has a slope of 0.015 [0.005] and a *p*-value of 0.0013 [<0.001]). The remarkable similarity in the three time series of each species testifies to the robustness of this measure of waviness given other differences among the data sets. For comparison, the waviness of the 500 hPa geostrophic flow from the NCEP time series was assessed by calculating the aggregate ALD of a set of five isohypses ranging from 576 to 528 dm (at 120 m intervals) chosen because they contain the maximum 500 hPa geostrophic wind throughout the cold season. The aggregate ALD is calculated by summing the ALD of each isohypse and dividing by 5. As seen in Figure 7, employment of isohypses at 500 hPa as a means of assessing the waviness of the midlatitude flow, as has recently been suggested by a number of studies (e.g., Barnes, 2013; Di Capua & Coumou, 2016; Francis & Vavrus, 2012; Overland et al., 2015; Screen & Simmonds, 2014), does not similarly testify to an increase in jet waviness. As suggested earlier, this incongruence is likely borne of the fact that lower tropospheric and diabatic processes exert a stronger influence on the flow at 500 hPa than at the tropopause. Interestingly, when a similar analysis is performed on a set of 5 isohypses ranging from 1,002 to 1,098 dm (at 240 m intervals) at 250 hPa, closer to the tropopause, the waviness is seen to increase over the 70-year NCEP time series ($p \ll 0.001$) (Figure 7).

Daily time series of the ALD of each jet in a single cold season can also be constructed and compared to one another, as shown, for example, in Figure 8 for the winter of 1990/91. Of interest in the present study is whether or not, and to what extent, the waviness of the two jets varies together. For the example season of 1990/91 the correlation between the two time series is quite low ($r = 0.2353$ for NCEP, 0.2217 for JRA-55, and 0.2481 for ERA5). In fact, the lack of even a modest correlation between the waviness of the two jets in a given cold season appears to be the rule rather than the exception. The two time series are correlated with magnitudes less than 0.3 in 52 of 70 NCEP cold seasons, 46 of 60 JRA-55 cold seasons, and 32 of 40 ERA5 cold seasons. Thus, despite synoptic evidence of episodic periods of substantial and impactful interaction between them (e.g., Bosart et al., 1996; Uccellini et al., 1984; Winters & Martin, 2014), it appears that throughout an average NH cold season the waviness of the two jet species evolves with a fair degree of independence. This characteristic is likely reflective of the fact that the two jets arise from quite different large-scale forcings.

The feature-based analysis method employed here to measure jet waviness relies upon calculation of the circulation along a collection of tropopause-level isertels. As described earlier, the isertel with the greatest circulation per unit length (e.g., the largest average $\bar{U}$) is deemed the core isertel. Thus, the *average $\bar{U}$ along the core isertel* on any given day represents the average jet speed for that species for that day. Time series of the seasonal average speeds of the subtropical and polar jet cores from each of the three reanalyzes are shown in Figure 9. A couple of characteristics of the analysis stand out. First, though the year-to-year variability in ERA5 is identical to that displayed by the nearly coincident NCEP/JRA-55 data, for both the subtropical and polar calculations, ERA5 data return lower values of the jet core speeds—by an average of 3.65 m s^{-1} for the STJ and 2.70 m s^{-1} for the POLJ. Second, focusing on the JRA-55 time series of both jets, the trends are very small indicating increases of just 0.6 m s^{-1} for the STJ and 1.0. m s^{-1} for the POLJ spread over 60 years with *p*-values of 0.1749 and 0.1483, respectively. Hoffman et al. (2019) showed that the zonally averaged NH jet in January 2017 was slightly slower in ERA5 than in the ERA-Interim (their Figures 3 and 4). They suggested that the higher spatial and temporal resolution of the ERA5 may account for the difference through improved representation of convective updrafts, gravity waves and other meso- to synoptic-scale features that can enhance mixing. The persistent discrepancy between the ERA5 and NCEP/JRA-55 jet core wind speeds in the present analysis may have similar origins.

Identification of the core isertel directly leads to calculation of the daily values of the equivalent latitude, essentially the zonally averaged latitude, of each jet core. Thus, another intriguing by-product of the analysis is the construction of time series of seasonal average equivalent latitudes of the subtropical and polar

Table 1
Integrated Seasonal Departures From Average ALD (Degrees) for Polar and Subtropical Jets From Each of the Three Reanalysis Data Sets

	POLJ			STJ		
	NCEP	*JRA-55*	*ERA5*	*NCEP*	*JRA-55*	*ERA5*
	-25.479	-31.211	-36.880	-41.237	-35.465	-43.334
	114.174	89.648	98.040	12.834	3.369	-1.809
	-45.440	-54.995	-64.633	2.379	-4.762	-7.651
	47.399	21.145	25.929	20.297	3.941	4.925
	13.270	10.836	4.961	11.548	2.428	0.349
	-7.471	-20.850	-29.738	33.853	27.473	25.678
	-34.958	-35.128	-47.171	18.302	5.476	2.906
	-25.341	-28.867	-41.351	-6.787	-14.986	-14.384
	-22.814	-46.551	-53.929	9.291	-1.551	1.136
	116.834	105.349	90.883	79.192	65.113	58.473
	29.288	15.952	13.369	34.377	11.742	8.882
	99.536	81.071	71.706	7.047	-8.538	-11.395
	93.481	65.564	58.102	-0.961	-7.381	-6.088
	121.620	111.992	104.084	9.279	-3.177	-4.539
	-10.179	-18.417	-33.067	11.187	-9.530	-11.452
	25.054	23.268	12.873	-9.582	-16.563	-15.908
	-37.879	-48.377	-55.943	-29.959	-37.803	-35.300
	7.530	8.194	16.938	33.652	22.315	21.628
	-0.703	-26.275	-32.642	-60.924	-66.183	-68.424
	46.407	23.446	8.379	55.309	51.668	43.310
	54.206	27.457	20.624	39.464	25.776	22.060
	-69.699	-93.429	-102.441	-1.283	-17.668	-17.196
	42.588	11.064	18.232	24.582	14.555	12.409
	-47.112	-66.039	-78.935	-35.310	-50.380	-45.714
	-3.058	-16.824	-21.979	29.378	20.351	9.074
	130.331	110.923	97.072	-22.081	-26.432	-28.831
	16.826	-12.040	-22.360	0.919	-9.158	-9.050
	55.886	32.809	9.000	19.413	10.058	8.043
	17.500	18.344	-8.009	48.975	39.542	38.413
	66.313	45.015	43.512	46.418	38.808	32.077
	-42.942	-142.652	-150.055	-70.569	-75.399	-71.700
	67.430	45.487	31.306	-9.666	-26.057	-23.790
	44.398	16.552	10.024	65.514	57.661	57.098
	6.021	-10.263	-33.913	13.182	1.827	-2.463
	63.316	37.177	30.714	39.152	25.792	23.384
	64.674	81.880	64.762	49.335	37.090	36.253
	-21.791	-13.414	-26.943	25.152	28.240	26.398
	15.433	29.617	17.488	14.313	-2.716	-3.949
	43.995	45.465	26.398	68.623	53.532	62.381

Notes. The analysis includes only the years common to all three data sets (1979–2017). Gray (light blue) shading indicates one of top five waviest (least wavy) seasons. The indicated year for each season includes December. See text for additional explanation.

Abbreviations: ALD, average latitudinal displacement; NCEP, National Centers for Environmental Prediction; POLJ, polar jet.
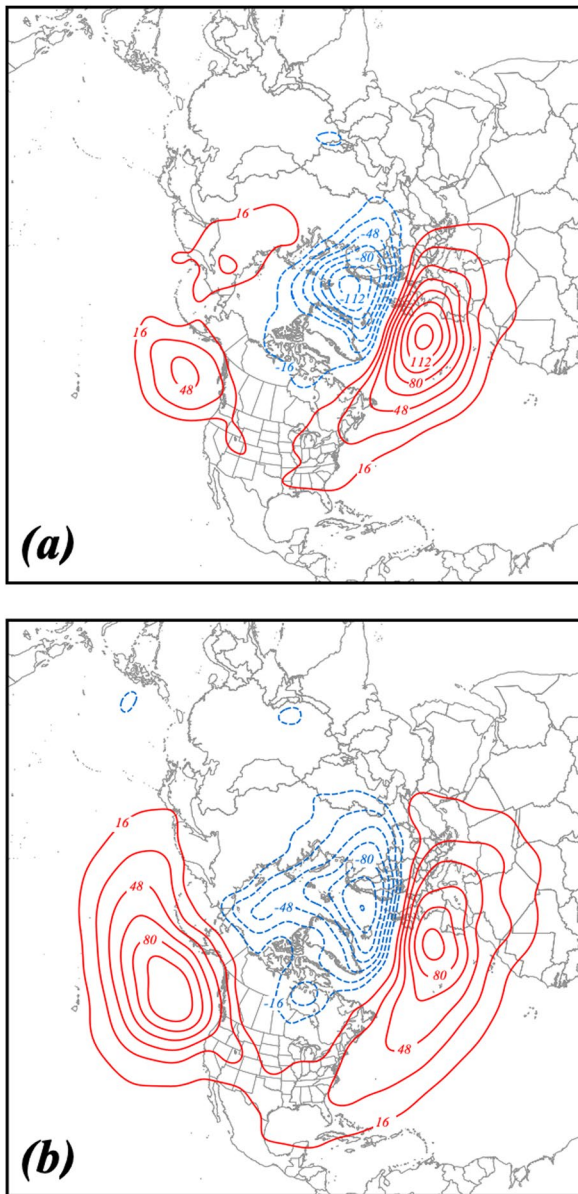
Figure 11. One thousand hectopascals height differences between composite waviest and least wavy (a) polar jet and (b) subtropical jet seasons constructed from the NCEP/NCAR reanalysis. See Table 1 for identification of the specific years comprising each composite. Positive (negative) height differences are in solid red (dashed blue) lines, labeled in m, and contoured every 16 m (−16 m) beginning at 16 m (−16 m). NCAR, National Center for Atmospheric Research; NCEP, National Centers for Environmental Prediction.

jet cores. Such time series, from each of the three reanalyzes, are shown in Figure 10. The trend lines through each time series are derived from the 60-year JRA-55 data. Very little change is suggested in the seasonally averaged latitude of the STJ (0.4° poleward increase over 60 years, $p = 0.222$). The polar jet, however, has crept northward at triple that rate and its trend line has a p-value of 0.008. Trend lines for the NCEP and ERA5 POLJs have p-values of 0.003 and 0.030, respectively.

3.2. Impact of Variability in Jet Waviness on NH Wintertime Circulation

Using the daily time series from each season, such as that in Figure 8, it is possible to identify the waviest and least wavy seasons for each jet species by simply summing the daily departures from average over the 90 days of each cold season. The list of integrated seasonal departures from average waviness for each species from each data set (for the overlapping years only) is shown in Table 1. From this list, the five waviest and five least wavy seasons for each species were identified. Composites of several variables from the waviest and least wavy POLJ and STJ seasons thus selected were constructed. In the subsequent analysis we show differences in each variable obtained by subtracting the least wavy from the waviest composite.

Figure 11a shows the 1,000 hPa geopotential height differences between seasons with the waviest and least wavy polar jets. Wavy polar jet seasons are attended by height anomalies reminiscent of the positive North Atlantic Oscillation (NAO) in the north Atlantic (Figure 11a). The height differences that exist between extremes of waviness of the subtropical jet share this positive NAO signal while exhibiting much more robust anomalous ridging centered on the Gulf of Alaska and extending from the west coast of North America to the dateline (Figure 11b).

Related to these lower tropospheric height differences are differences in the 300 hPa zonal wind. In the north Atlantic, the wavy polar jet seasons are characterized by a poleward displacement of the jet axis and a weakening of the zonal wind in a band stretching across the basin from the Carolina coast to Iberia and the Mediterranean. In the Pacific basin, wavy polar jet years appear to have little influence on the Pacific jet along nearly the length of its climatological axis (Figure 12a). The influence of subtropical jet variability on the circulation changes in the north Atlantic is quite similar while in the Pacific basin wavy subtropical jet seasons encourage a poleward displacement of the jet over the Bering Sea and Gulf of Alaska and a broadly weaker flow equatorward of the climatological jet position in the central Pacific (Figure 12b). Such a distribution of anomalies is similar to that associated with north Pacific jet retractions (Jaffe et al., 2011) which represent one phase of the leading mode of jet variability in the basin (Athanasiadis et al., 2010).

The circulation differences engendered by the inter-seasonal variability in jet waviness are apparently not confined to the troposphere. Associated modulations to the lower stratospheric polar vortex are illustrated in Figure 13. Wavy polar jet years are associated with an intensified polar vortex over the Canadian Archipelago rung by light height rises at middle latitudes (Figure 13a). Lower stratospheric circulation changes arising from inter-seasonal variation in the waviness of the subtropical jet are quite different with the vortex core displaced much farther west in wavy STJ years while pronounced ridging occurs over Scandinavia (Figure 13b).
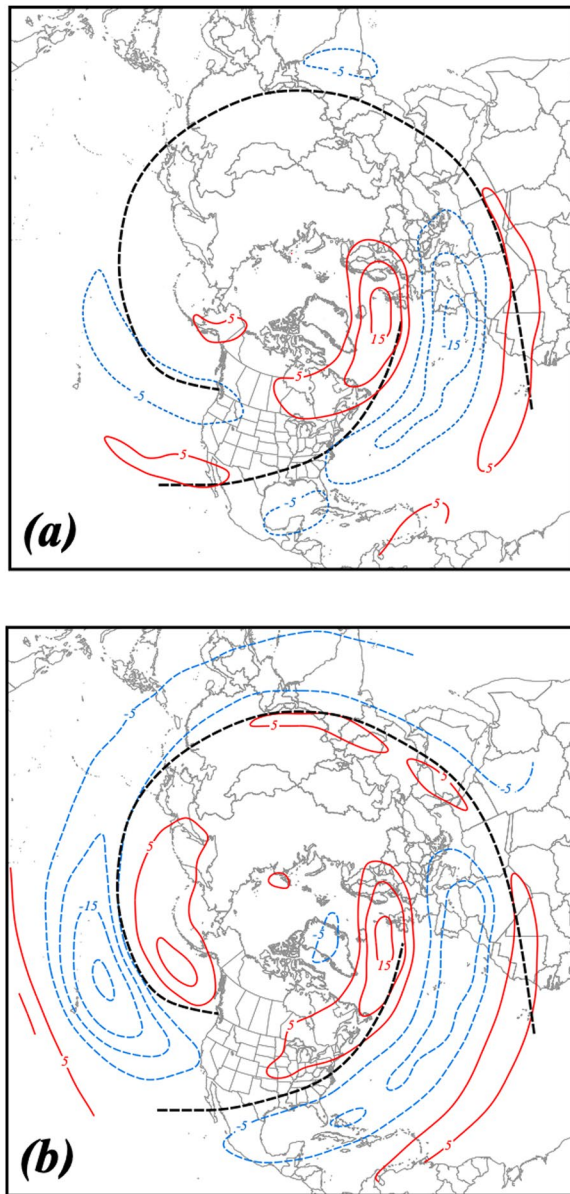
Figure 12. Three hundred hectopascals zonal wind differences between composite waviest and least wavy (a) polar jet and (b) subtropical jet seasons constructed from the NCEP/NCAR reanalysis. See Table 1 for identification of the specific years comprising each composite. Positive (negative) wind differences are in solid red (dashed blue) lines, labeled in m s^{-1}, and contoured every 5 m s^{-1} (-5 m s^{-1}) beginning at 5 m s^{-1} (-5 m s^{-1}). Black dashed lines represent climatological axes of the DJF 300 hPa zonal wind. NCAR, National Center for Atmospheric Research; NCEP, National Centers for Environmental Prediction.

4. Summary

The analysis presented here focuses on observed morphological aspects of the NH tropopause-level jet streams during boreal winter (DJF) as portrayed in three different reanalysis data sets covering parts of the last six and a half decades. Based upon the definitions of the polar and subtropical jets offered by Christensen et al. (2017), the analysis identifies a "core isertel" along which the circulation per unit length is maximized in the separate polar (315:330K) and subtropical (340:355K) isentropic layers for each day in the three time series. Such a core isertel represents an analytical proxy for the respective jet cores. Calculation of the hemispheric average latitudinal displacement of the core isertel from its equivalent latitude is, therefore, a robust, feature-based metric of the waviness of each species of jet. The analysis reveals that both jets are becoming systematically wavier while exhibiting no trends in their average speeds. Examination of the daily time series of waviness of the two jets strongly suggests that one's undulatory nature develops largely in isolation from the other. Additionally, while both jet cores are creeping toward the pole over time, only the POLJ encroachment, at three times the rate of the STJ, is statistically significant.

The poleward shift of the POLJ revealed here is consistent with observations of systematic poleward shifts in midlatitude cloud fields over the past several decades as shown in the analyses of Bender et al. (2012), Eastman and Warren (2013) and Norris et al. (2016). It is also in line with recent analyses by Archer and Caldeira (2008) and Peña-Ortiz et al. (2013) that have identified a poleward migration of the NH wintertime jets. Importantly, however, in both of those observational studies distinction between the POLJ and STJ was not emphasized. Additionally, modeling evidence suggests that increasing greenhouse gases will force the NH midlatitude jet poleward in the 21st century (e.g., Barnes & Polvani, 2013; Lorenz & DeWeaver, 2007; Simpson et al., 2014). In fact, in their analysis of CMIP5 model output, Barnes and Polvani (2013) found that the NH jet shifted ~1° poleward by the end of the century while its core speed remained constant. Such behavior is consistent with the results of the present observational analysis.

The limited poleward migration of the STJ suggested by the present analysis is somewhat out of step with a collection of other observational studies (e.g., Archer & Caldeira, 2008; Manney & Hegglin, 2018; Peña-Ortiz et al., 2013; Seidel et al., 2007) in which a more rapid northward advance is suggested. However, consensus on this characteristic of the STJ does not exist as recent hemispheric and regional analyses, by Maher et al. (2019) and Luna-Niño et al. (2020), respectively, find little poleward advance of the STJ. The Maher et al. (2019) jet identification method focused on finding maxima in $|\nabla\theta|$ on the dynamic tropopause and so bears some similarity to that used here. It is thus suggested that the method of jet identification can exert a notable influence on the analysis of changes in jet characteristics.

Trends in jet core wind speeds, obtained either from observational analyses or model simulations, also exhibit little consensus at present. The observational analyses of Archer and Caldeira (2008) and Peña-Ortiz et al. (2013) suggest a weakening and a strengthening, respectively, of the NH wintertime jet while the modeling results of Lorenz and DeWeaver (2007) predict a strengthening of the tropospheric zonal jets. The present analysis finds no trend in jet core wind speed for either jet species and so offers little hope for
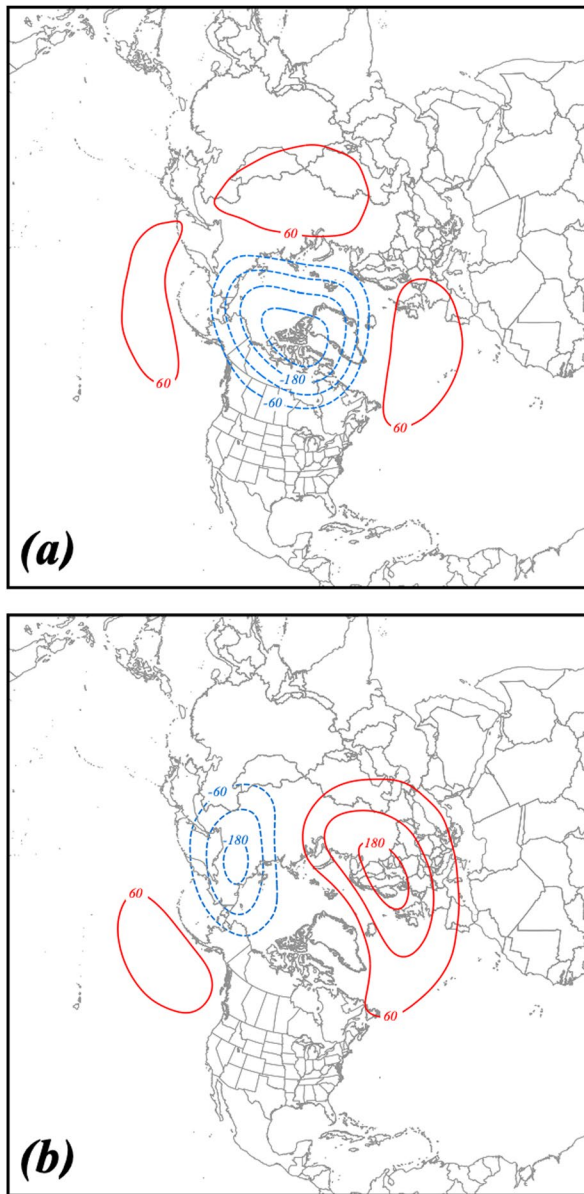
resolving this conundrum. The analysis revealed that wavy POLJ and STJ years tend to be associated with height anomalies similar to those of a positive NAO in the north Atlantic. Thus, the fact that the jets have become systematically wavier since ~1960 might lead to an expectation of a positive trend in the NAO over the same interval. In fact, the trend in the seasonal (DJF) NAO was systematically positive from ~1960 to the mid-1990s when it began a period of decline that lasted through ~2010 (Based upon the Hurrell, 1995, PC-based North Atlantic Oscillation Index available at https://climatedataguide.ucar.edu/climate-data/hurrell-north-atlantic-oscillation-nao-index-pc-based). The discrepancy between expectation and reality may be a function of jet definition, the fact that the present analysis only considers the high frequency waviness, or the acknowledged influence of the East Atlantic (EA) pattern on the latitude and speed of the north Atlantic jet (Woollings & Blackburn, 2012; Woollings et al., 2010). Further consideration of this issue is left to future work.

Though the aim of this study is to document, rather than diagnose, increasing jet waviness, prior work has considered the dynamical interaction between increased waviness and poleward migration of the jets. A number of investigators (e.g., Benedict et al., 2004; Martius et al., 2007; Rivière, 2009; Rivière & Orlanski, 2007; Strong & Magnusdottir, 2008; Thorncroft et al., 1993; Woollings et al., 2008) have examined the poleward momentum flux characteristic of certain configurations of the large scale flow. These analyses have concluded that individual synoptic-scale eddies can play an important role in the formation of large-scale flow anomalies through wave breaking. Vallis and Gerber (2008) have suggested that high impact teleconnections such as the North Atlantic Oscillation (NAO), the Pacific North America pattern (PNA), and the annular modes are fundamentally related to fluctuations in the latitude and amplitude of the tropopause-level jets. Introduction of the LC1/LC2 life cycle dichotomy by Thorncroft et al. (1993) represented a recognition that anticyclonic (LC1) and cyclonic (LC2) wave breaking lay at the heart of the interaction of eddies with the larger scale flow. When anticyclonic wave breaking occurs near the jet core, the jet is pushed poleward in response to the associated distribution of momentum fluxes. Framed in terms of the PV gradient, Rivière (2009) concluded that a higher latitude jet is more likely to experience anticyclonic wavebreaks which would, in turn, encourage further poleward displacement. If the increased waviness reported here has been manifest as an increase in the frequency of positively tilted waves, then the attendant poleward migration of the jets may bear a direct dynamical link to the waviness. Examination of this potential connection, dependent on construction of an objective method for identifying the tilt of the waves, following the work of Wernli and Sprenger (2007) and Martius et al. (2008), is a subject of ongoing research.

Figure 13. Fifty hectopascals height differences between composite waviest and least wavy (a) polar jet and (b) subtropical jet seasons constructed from the NCEP/NCAR reanalysis. See Table 1 for identification of the specific years comprising each composite. Positive (negative) height differences are in solid red (dashed blue) lines, labeled in m and contoured every 60 m (−60 m) beginning at 60 m (−60 m). NCAR, National Center for Atmospheric Research; NCEP, National Centers for Environmental Prediction.

Equally unknown in the wake of the present analysis is the role of the tropics in forcing the observed increased waviness of the subtropical jet. A recent analysis of the subtropical jet by Martius (2014) considered the interaction of the tropics and extratropics with the jet from the perspective of trajectory analysis. She showed that air parcels that ended up in the jet over Africa (East Asia/western Pacific) ascended over South America (Indian Ocean and the Maritime Continent) before following an anticyclonic path toward the jet. The analysis showed that the wintertime Hadley circulation is zonally asymmetric connecting tropical convection in localized regions to segments of the jet. Whether or not the increased waviness of the subtropical jet is directly related to changes in such tropical convective forcing is not known though a recent analysis by Röthlisberger et al. (2018) suggests a connection.

The analysis methodology introduced here has been applied hemispherically but could equally be employed in regional analyses. Such a regional analysis of the 500 hPa flow over North America and its relation to Arctic amplification and hemispheric snow cover was recently performed by Vavrus et al. (2017). A primary motivation for shrinking the analysis domain was their suspicion that doing so would enhance the strength of the desired signal. Indeed, Di Capua and Coumou (2016) found that regional trends in their meandering index were 2–3 times larger than those observed over the full hemisphere. Tracking regional trends in the average latitudinal displacement of the core isertel would identify which regions are most strongly contributing to the hemispheric trend identified here. Such an analysis would likely also provide a more detailed sense of the physical connections between the parade of weather systems and the increased waviness of the jets.

Finally, use of reanalysis data sets to determine climatological trends can be problematic for a number of reasons including changing data types and volumes as well as biases in assimilation systems as suggested by Bengtsson et al. (2004). The results presented here rely on application of an analysis scheme to three quite different reanalysis data sets, each with its own advantages and disadvantages. The remarkably similar signals arising from these heterogeneous inputs suggests a robustness to the underlying signal that this analysis has sought to uncover. A convincing alternative assessment of these results would result from applying the same analysis method to output from 20th century GCM runs in the CMIP5 or CMIP6 suites. Such work is currently ongoing.

Data Availability Statement

NCEP Reanalysis data provided by the NOAA/OAR/ESRL PSL, Boulder, CO and available at https://psl.noaa.gov/data/gridded/data.ncep.reanalysis.html. JRA-55 data available from the Research Data Archive at the National Center for Atmospheric Research (https://rda.ucar.edu/datasets/ds628.0/). ERA5 data available at Copernicus Climate Change Service Climate Data Store (CDS), https://cds.climate.copernicus.eu/cdsapp#!/home.

References

Archer, C. L., & Caldeira, K. (2008). Historical trends in the jet stream. *Geophysical Research Letters*, *35*(8). https://doi.org/10.1029/2008gl033614

Athanasiadis, P. J., Wallace, J. M., & Wettstein, J. J. (2010). Patterns of wintertime jet stream variability and their relation to the storm tracks. *Journal of the Atmospheric Sciences*, *67*, 1361–1381. https://doi.org/10.1175/2009jas3270.1

Barnes, E. A. (2013). Revisiting the evidence linking Arctic amplification to extreme weather in midlatitudes. *Geophysical Research Letters*, *40*, 4734–4739. https://doi.org/10.1002/grl.50880

Barnes, E. A., & Polvani, L. (2013). Response of the midlatitude jets, and of their variability, to increased greenhouse gases in the CMIP5 models. *Journal of Climate*, *26*, 7117–7135.

Barnes, E. A., & Screen, J. A. (2015). The impact of Arctic warming on the midlatitude jet-stream: Can it? Has it? Will it? *WIREs Climate Change*, *6*, 277–286. https://doi.org/10.1002/wcc.337

Bender, F. A.-M., Ramanathan, V., & Tselioudis, G. (2012). Changes in extratropical storm track cloudiness 1983-2008: Observational support for a poleward shift. *Climate Dynamics*, *38*, 2037–2053. https://doi.org/10.1007/s00382-011-1065-6

Benedict, J. J., Lee, S., & Feldstein, S. B. (2004). Synoptic view of the North Atlantic oscillation. *Journal of the Atmospheric Sciences*, *61*, 121–144. https://doi.org/10.1175/1520-0469(2004)061<0121:svotna>2.0.co;2

Bengtsson, L., Hagemann, S., & Hodges, K. I. (2004). Can climate trends be calculated from reanalysis data? *Journal of Geophysical Research*, *109*(D11). https://doi.org/10.1029/2004jd004536

Blackport, R., & Screen, J. A. (2020). Insignificant effect of Arctic amplification on the amplitude of midlatitude atmospheric waves. *Science advances*, *6*(8). https://doi.org/10.1126/sciadv.aay2880

Bosart, L. F., Hakim, G. J., Tyle, K. R., Bedrick, M. A., Bracken, W. E., Dickinson, M. J., & Schultz, D. M. (1996). Large-scale antecedent conditions associated with the 12-14 March 1993 cyclone ("Superstorm '93") over Eastern North America. *Monthly Weather Review*, *124*, 1865–1891. https://doi.org/10.1175/1520-0493(1996)124<1865:lsacaw>2.0.co;2

Bretherton, F. P. (1966). Critical layer instability in baroclinic flows. *Quarterly Journal of the Royal Meteorological Society*, *92*, 325–334. https://doi.org/10.1002/qj.49709239302

Chen, G., Lu, J., Burrows, D. A., & Leung, L. R. (2015). Local finite-amplitude wave activity as an objective diagnostic of midlatitude extreme weather. *Geophysical Research Letters*, *42*, 10952–10960. https://doi.org/10.1002/2015gl066959

Christenson, C. E., Martin, J. E., & Handlos, Z. J. (2017). A synoptic climatology of Northern Hemisphere, cold season polar and subtropical jet superposition events. *Journal of Climate*, *30*, 7231–7246. https://doi.org/10.1175/jcli-d-16-0565.1

Copernicus Climate Change Service (C3S). (2017). *ERA5: Fifth generation of ECMWF atmospheric reanalyses of the global climate*. Copernicus Climate Change Service Climate Data Store (CDS). Retrieved from https://cds.climate.copernicus.eu/cdsapp#!/home

Cunningham, P., & Keyser, D. (2004). Dynamics of jet streaks in a stratified quasi-geostrophic atmosphere: Steady-state representations. *Quarterly Journal of the Royal Meteorological Society*, *130*, 1579–1609. https://doi.org/10.1256/qj.03.35

Davies, H. C., & Rossa, A. M. (1998). PV frontogenesis and upper-tropospheric fronts. *Monthly Weather Review*, *126*, 1528–1539. https://doi.org/10.1175/1520-0493(1998)126<1528:pfautf>2.0.co;2

Davis, C. A., & Emanuel, K. A. (1991). Potential vorticity diagnostics of cyclogenesis. *Monthly Weather Review*, *119*, 1929–1953. https://doi.org/10.1175/1520-0493(1991)119<1929:pvdoc>2.0.co;2

Defant, F., & Taba, H. (1957). The threefold structure of the atmosphere and the characteristics of the tropopause. *Tellus*, *9*, 259–274. https://doi.org/10.3402/tellusa.v9i3.9112

desJardins, M. L., Brill, K. F., & Schotz, S. S. (1991). *Use of GEMPAK on UNIX workstations* (pp. 449–453). Paper presented at Seventh Conference on Interactive Information Processing Systems for Meteorology, Oceanography, and Hydrology, American Meteorological Society.

Di Capua, G., & Coumou, D. (2016). Changes in meandering of the Northern Hemisphere circulation. *Environmental Research Letters*, *11*, 094028, 094028. https://doi.org/10.1088/1748-9326/11/9/094028

Eastman, R., & Warren, S. G. (2013). A 39-yr survey of cloud changes from land stations worldwide 1971-2009: Long-term trends, relation to aerosols, and expansion of the tropical belt. *Journal of Climate*, *26*, 1286–1303. https://doi.org/10.1175/jcli-d-12-00280.1

Ertel, H. (1942). Ein Neuer hydrodynamischer Wirbelsatz. *Meteorologische Zeitschrift*, *59*, 271–281.

Francis, J. A. (2017). Why are Arctic linkages to extreme weather still up in the air?. *Bulletin of the American Meteorological Society*, *98*, 2551–2557. https://doi.org/10.1175/bams-d-17-0006.1

Francis, J. A., Skific, N., & Vavrus, S. J. (2018). North American weather regimes are becoming more persistent: Is Arctic amplification a factor? *Geophysical Research Letters*, *45*, 11414–11422. https://doi.org/10.1029/2018gl080252

Francis, J. A., & Vavrus, S. J. (2012). Evidence linking Arctic amplification to extreme weather in mid-latitudes. *Geophysical Research Letters*, *39*, L06801. https://doi.org/10.1029/2012GL051000

Francis, J. A., & Vavrus, S. J. (2015). Evidence for a wavier jet stream in response to rapid Arctic warming. *Environmental Research Letters*, *10*, 014005, 014005. https://doi.org/10.1088/1748-9326/10/1/014005

Held, I. M. (1975). Momentum transport by quasi-geostrophic eddies. *Journal of the Atmospheric Sciences*, *32*, 1494–1497. https://doi.org/10.1175/1520-0469(1975)032<1494:mtbqge>2.0.co;2

Held, I. M., & Hou, A. Y. (1980). Nonlinear axially symmetric circulations in a nearly inviscid atmosphere. *Journal of the Atmospheric Sciences*, *37*, 515–533. https://doi.org/10.1175/1520-0469(1980)037<0515:nascia>2.0.co;2

Hoffman, L. G., Gunther, D., Li, O., Stein, X., Wu, S., Greissbach, Y., et al. (2019). From ERA-Interim to ERA5: The considerable impact of ECMWF's next-generation reanalysis on Lagrangian transport simulations. *Atmospheric Chemistry and Physics*, *19*, 3097–3124.

Hoskins, B. J., & Berrisford, P. (1988). A potential vorticity perspective of the storm of 15-16 October 1987. *Weather*, *43*, 122–129. https://doi.org/10.1002/j.1477-8696.1988.tb03890.x

Hoskins, B. J., McIntyre, M. E., & Robertson, A. W. (1985). On the use and significance of isentropic potential vorticity maps. *Quarterly Journal of the Royal Meteorological Society*, *111*, 877–946.

Huang, C. S. Y., & Nakamura, N. (2016). Local finite-amplitude wave activity as a diagnostic of anomalous weather events. *Journal of the Atmospheric Sciences*, *73*, 211–229. https://doi.org/10.1175/jas-d-15-0194.1

Hurrell, J. W. (1995). Decadal trends in the north Atlantic oscillation: Regional temperatures and precipitation. *Science*, *269*, 676–679. https://doi.org/10.1126/science.269.5224.676

Jaffe, S. C., Martin, J. E., Vimont, D. J., & Lorenz, D. J. (2011). A synoptic climatology of episodic, subseasonal retractions of the Pacific jet. *Journal of Climate*, *24*, 2846–2860. https://doi.org/10.1175/2010jcli3995.1

Kalnay, E., Kanamitsu, M., Kistler, R., Collins, W., Deaven, D., Gandin, L., et al. (1996). The NCEP/NCAR 40-year reanalysis project. *Bulletin of the American Meteorological Society*, *77*, 437–471. https://doi.org/10.1175/1520-0477(1996)077<0437:tnyrp>2.0.co;2

Kistler, R., Collins, W., Saha, S., White, G., Woollen, J., Kalnay, E., et al. (2001). The NCEP-NCAR 50-year reanalysis: Monthly means CD-ROM and documentation. *Bulletin of the American Meteorological Society*, *82*, 247–267. https://doi.org/10.1175/1520-0477(2001)082<0247:tnnyrm>2.3.co;2

Kobayashi, S. Y., Ota, Y. Harada, A. Ebita, M. Moriya, H. Onoda, K, et al. (2015). The JRA-55 reanalysis: General specifications and basic characteristics. *Journal of the Meteorological Society of Japan*, *93*, 5–48. https://doi.org/10.2151/jmsj.2015-001

Koch, P., Wernli, H., & Davies, H. C. (2006). An event-based jet-stream climatology and typology. *International Journal of Climatology*, *26*, 283–301. https://doi.org/10.1002/joc.1255

Kunz, A., Sprenger, M., & Wernli, H. (2015). Climatology of potential vorticity streamers and associated isentropic transport pathways across PV gradient barriers. *Journal of Geophysical Research: Atmospheres*, *120*, 3802–3821. https://doi.org/10.1002/2014JD022615

Limbach, S., Schömer, E., & Wernli, H. (2012). Detection, tracking and event localization of jet stream features in 4-D atmospheric data. *Geoscientific Model Development*, *5*, 457–470. https://doi.org/10.5194/gmd-5-457-2012

Lorenz, D. J., & DeWeaver, E. T. (2007). Tropopause height and zonal wind response to global warming in the IPCC scenario integrations. *Journal of Geophysical Research*, *112*(D10). https://doi.org/10.1029/2006jd008087

Luna-Niño, R., Cavazos, T., Torres-Alvarez, J. A., Giorgi, F., & Coppola, E. (2020). Interannual variability of the boreal winter subtropical jet stream and teleconnections over the CORDEX-CAM domain during 1980-2010. *Climate Dynamics*, *55*, 1–24.

Maher, P., Kelleher, M. E., Sansom, P. G., & Methven, J. (2019). Is the subtropical jet shifting poleward? *Climate Dynamics*, *54*, 1741–1759. https://doi.org/10.1007/s00382-019-05084-6

Manney, G. L., & Hegglin, M. I. (2018). Seasonal and regional variations of long-term changes in upper-tropospheric jets from reanalyses. *Journal of Climate*, *31*, 423–448. https://doi.org/10.1175/jcli-d-17-0303.1

Manney, G. L., Hegglin, M. I., Daffer, W. H., Santee, M. L., Ray, E. A., Pawson, S., et al. (2011). Jet characterization in the upper troposphere/lower stratosphere (UTLS): Applications to climatology and transport studies. *Atmospheric Chemistry and Physics*, *11*, 6115–6137. https://doi.org/10.5194/acp-11-6115-2011

Martineau, P., Chen, G., & Burrows, D. A. (2017). Wave events: Climatology, trends, and relationship to Northern Hemisphere winter blocking and weather extremes. *Journal of Climate*, *30*, 5675–5697. https://doi.org/10.1175/jcli-d-16-0692.1

Martius, O. (2014). A Lagrangian analysis of the Northern Hemisphere subtropical jet. *Journal of the Atmospheric Sciences*, *71*, 2354–2369. https://doi.org/10.1175/jas-d-13-0329.1

Martius, O., Schwierz, C., & Davies, H. C. (2007). Breaking waves at the tropopause in the wintertime Northern Hemisphere: Climatological analyses of the orientation and the theoretical LC1/2 classification. *Journal of the Atmospheric Sciences*, *64*, 2576–2592. https://doi.org/10.1175/jas3977.1

Martius, O., Schwierz, C., & Davies, H. C. (2008). Far-upstream precursors of heavy precipitation events on the Alpine south-side. *Quarterly Journal of the Royal Meteorological Society*, *134*, 417–428. https://doi.org/10.1002/qj.229

Miller, R. L., Schmidt, G. A., & Shindell, D. T. (2006). Forced annular variations in the 20th century Intergovernmental Panel on Climate Change Fourth Assessment Report models. *Journal of Geophysical Research*, 111. D18101. https://doi.org/10.1029/2005JD006323

Morgan, M. C., & Nielsen-Gammon, J. W. (1998). Using tropopause maps to diagnose midlatitude weather systems. *Monthly Weather Review*, *126*, 2555–2579. https://doi.org/10.1175/1520-0493(1998)126<2555:utmtdm>2.0.co;2

Norris, J. R., Allen, R. J., Evan, A. T., Zelinka, M. D., O'Dell, C. W., & Klein, S. A. (2016). Evidence for climate change in the satellite cloud record. *Nature*, *536*, 72–75. https://doi.org/10.1038/nature18273. https://doi.org/10.1038/nature18273

Overland, J., Francis, J. A., Hall, R., Hanna, E., Kim, S.-J., & Vihma, T. (2015). The melting arctic and midlatitude weather patterns: Are they connected? *Journal of Climate*, *28*, 7917–7932. https://doi.org/10.1175/jcli-d-14-00822.1

Panetta, R. L. (1993). Zonal jets in wide baroclinically unstable regions: Persistence and scale selection. *Journal of the Atmospheric Sciences*, *50*, 2073–2106. https://doi.org/10.1175/1520-0469(1993)050<2073:zjiwbu>2.0.co;2

Peña-Ortiz, C., Gallego, D., Ribera, P., Ordonez, P., & Alvarez-Castro, M. D. C. (2013). Observed trends in the global jet stream characteristics during the second half of the 20th century. *Journal of Geophysical Research: Atmospheres*, *118*, 2702–2713. https://doi.org/10.1002/jgrd.50305

Rhines, P. B. (1975). Waves and turbulence on a beta-plane. *Journal of Fluid Mechanics*, *69*, 417–443. https://doi.org/10.1017/s0022112075001504

Rivière, G. (2009). Effect of latitudinal variations in low-level baroclinicity on eddy life cycles and upper-tropospheric wave-breaking processes. *Journal of the Atmospheric Sciences*, *66*, 1569–1592. https://doi.org/10.1175/2008jas2919.1

Rivière, G., & Orlanski, I. (2007). Characteristics of the Atlantic storm-track eddy activity and its relation with the North Atlantic Oscillation. *Journal of the Atmospheric Sciences*, *64*, 241–266. https://doi.org/10.1175/jas3850.1

Röthlisberger, M., Martius, O., & Wernli, H. (2018). Northern Hemisphere Rossby wave initiation events on the extratropical jet-A climatological analysis. *Journal of Climate*, *31*, 743–760. https://doi.org/10.1175/jcli-d-17-0346.1

Santer, B. D., Hnilo, J. J., Wigley, T. M. L., Boyle, J. S., Doutriaux, C., Fiorino, M., et al. (1999). Uncertainties in observationally based estimates of temperature change in the free atmosphere. *Journal of Geophysical Research*, *104*, 6305–6333. https://doi.org/10.1029/1998jd200096

Scheimann, R., Lüthi, D., & Schär, C. (2009). Seasonality and interannual variability of the westerly jet in the Tibetan Plateau region. *Journal of Climate*, *22*, 2940–2957.

Screen, J. A., & Simmonds, I. (2010). The central role of diminishing sea ice in recent Arctic temperature amplification. *Nature*, *464*, 1334–1337. https://doi.org/10.1038/nature09051

Screen, J. A., & Simmonds, I. (2013). Exploring links between Arctic amplification and mid-latitude weather. *Geophysical Research Letters*, *40*, 959–964. https://doi.org/10.1002/grl.50174

Screen, J. A., & Simmonds, I. (2014). Amplified mid-latitude planetary waves favour particular regional weather extremes. *Nature Climate Change*, *4*, 704–709. https://doi.org/10.1038/nclimate2271

Seidel, D. J., & Randel, W. L. (2007). Recent widening of the tropical belt: Evidence from tropopause observations. *Journal of Geophysical Research*, *112*(D20). https://doi.org/10.1029/2007jd008861

Serreze, M. C., Barrett, A. P., Stroeve, J. C., Kindig, D. N., & Holland, M. M. (2009). The emergence of surface-based Arctic amplification. *The Cryosphere*, *3*, 11–19. https://doi.org/10.5194/tc-3-11-2009

Simpson, I. R., Shaw, T. A., & Seager, R. (2014). A diagnosis of the seasonally and longitudinally varying midlatitude circulation response to global warming. *Journal of the Atmospheric Sciences*, *71*, 2489–2515. https://doi.org/10.1175/jas-d-13-0325.1

Strong, C., & Magnusdottir, G. (2008). Tropospheric Rossby wave breaking and the NAO/NAM. *Journal of the Atmospheric Sciences*, *65*, 2861–2876. https://doi.org/10.1175/2008jas2632.1

Sturaro, G. (2003). A closer look at the climatological discontinuities present in the NCEP/NCAR reanalysis temperature due to the introduction of satellite data. *Climate Dynamics*, *21*, 309–316. https://doi.org/10.1007/s00382-003-0334-4

Swart, N. C., & Fyfe, J. C. (2012). Observed and simulated changes in the Southern Hemisphere surface westerly wind-stress. *Geophysical Research Letters*, *39*, L16711. https://doi.org/10.1029/2012GL052810

Thorncroft, C. D., Hoskins, B. J., & McIntyre, M. E. (1993). Two paradigms of baroclinic-wave life-cycle behaviour. *Quarterly Journal of the Royal Meteorological Society*, *119*, 17–55. https://doi.org/10.1002/qj.49711950903

Uccellini, L. W., Kocin, P. J., Petersen, R. A., Wash, C. H., & Brill, K. F. (1984). The presidents' day cyclone of 18-19 February 1979: Synoptic overview and analysis of the subtropical jet streak influencing the pre-cyclogenetic period. *Monthly Weather Review*, *112*, 31–55. https://doi.org/10.1175/1520-0493(1984)112<0031:tpdcof>2.0.co;2

Vallis, G. K., & Gerber, E. P. (2008). Local and hemispheric dynamics of the North Atlantic Oscillation, annular patterns and the zonal index. *Dynamics of Atmospheres and Oceans*, *44*, 184–212. https://doi.org/10.1016/j.dynatmoce.2007.04.003

Vavrus, S. J. (2018). The influence of Arctic amplification on mid-latitude weather and climate. *Current Climate Change Reports*, *4*, 238–249. https://doi.org/10.1007/s40641-018-0105-2

Vavrus, S. J., Wang, F., Martin, J. E., Francis, J. A., Peings, Y., & Cattiaux, J. (2017). Changes in North American atmospheric circulation and extreme weather: Influence of Arctic amplification and Northern Hemisphere snow cover. *Journal of Climate*, *30*, 4317–4333. https://doi.org/10.1175/jcli-d-16-0762.1

Wernli, H., & Sprenger, M. (2007). Identification and ERA-15 climatology of potential vorticity streamers and cutoffs near the extratropical tropopause. *Journal of the Atmospheric Sciences*, *64*, 1569–1586. https://doi.org/10.1175/jas3912.1

Winters, A. C., & Martin, J. E. (2014). The role of a polar/subtropical jet superposition in the May 2010 Nashville Flood. *Weather and Forecasting*, *29*, 954–974. https://doi.org/10.1175/waf-d-13-00124.1

Woollings, T., & Blackburn, M. (2012). The north Atlantic jet stream under climate change and its relation to the NAO and EA patterns. *Journal of Climate*, *25*, 886–902. https://doi.org/10.1175/jcli-d-11-00087.1

Woollings, T., Hannachi, A., & Hoskins, B. (2010). Variability of the North Atlantic eddy-driven jet stream. *Quarterly Journal of the Royal Meteorological Society*, *136*, 856–868. https://doi.org/10.1002/qj.625

Woollings, T., Hoskins, B., Blackburn, M., & Berrisford, P. (2008). A new Rossby wave-breaking interpretation of the North Atlantic Oscillation. *Journal of the Atmospheric Sciences*, *65*, 609–626. https://doi.org/10.1175/2007jas2347.1

Yin, J. H. (2005). A consistent poleward shift of the storm tracks in simulations of 21st century climate. *Geophysical Research Letters*, *32*, L18701. https://doi.org/10.1029/2005GL023684